

DreamSR: Towards Ultra-High-Resolution Image Super-Resolution via a Receptive-Field Enhanced Diffusion Transformer

Qingji Dong¹ Hang Dong^{1*} Mingqin Chen¹ Rui Zhang¹ Yitong Wang¹
¹ ByteDance Inc.

Abstract

Large-scale pre-trained diffusion models have been extensively adopted for real-world image Super-Resolution because of their powerful generative priors through textual guidance. However, when super-resolving high-resolution images with patch-wise inference strategy, most existing diffusion-based SR methods tend to suffer from over-generation, due to the misalignment between the global prompt from LR image and the incomplete semantic information of local patches during each inference step. On the other hand, most existing methods also failed to generate detailed texture in local patches due to the overemphasis on global generation capabilities in network designs and training strategies. To address this issue, we present DreamSR, a novel SR model that suppresses local over-generation and improves fine-detail synthesis, thereby achieving visually faithful results with ultra-high-quality details. Specifically, we propose a dual-branch MM-ControlNet, where the ControlNet generates local textual feature with patch-level prompts while the pre-trained DiT provides global textual feature with global prompts, thereby mitigating over-generation and ensuring semantic consistency across patches. We also design a comprehensive training strategy with stage-specific data processing pipelines and a Receptive-Field Enhancement strategy, enhancing the model’s capability to capture patch information and effectively restore local textures. Extensive experiments demonstrate that DreamSR outperforms state-of-the-art methods, providing high-quality SR results. Code and model are available at <https://github.com/jerrydong0219/DreamSR>.

1. Introduction

Real-world Image Super-Resolution (Real-ISR) aims to reconstruct high-resolution (HR) images from low-resolution (LR) inputs with unknown degradation. This task requires the model not only to effectively remove diverse degradations but also to generate perceptually realistic details, es-

pecially in challenging ultra-high-resolution ($\geq 4K$) scenarios. Recent text-to-image (T2I) diffusion-based Real-ISR approaches [68, 70] significantly outperform earlier GAN-based methods [6, 29, 56], owing to the appropriate selection of generative prior and the effective incorporation of these priors into Real-ISR. However, these methods still face limitations; either the selection of pre-trained priors is suboptimal, or the pre-trained image priors are insufficiently exploited. The problem becomes particularly pronounced in ultra-high-resolution scenarios, where patch-wise inference [2] is necessary due to computational constraints. During patch-wise inference, the limited semantic information within each patch conflicts with the global textural guidance derived from the LR image, resulting in undesired artifacts (over-generation). Trivially employing local prompts fails to reconstruct fine textures (under-generation), as such local prompts are inadequate to activate the full generative capacity of the pre-trained model.

In this paper, we propose DreamSR, a method tailored for ultra-high-resolution image reconstruction with patch-wise inference, aiming at fully leveraging the pre-trained T2I generative prior. Specifically, we employ FLUX [3] as our backbone due to its unified architecture, which avoids the split of generative priors across separate base and refiner models, i.e., SDXL [43]. To address the aforementioned over-generation and under-generation issues, we introduce a dual-branch network architecture Patch Context aware MM-ControlNet. In this design, one ControlNet branch utilizes local prompts to capture visual features of local patches, while the fixed DiT backbone leverages global prompts to fully activate the pre-trained generative prior. Based on the proposed architecture, we design a two-stage inference framework consisting of degradation removal and texture generation. We define the multi-step denoising process of the diffusion model as the texture generation stage, which focuses on refining high-frequency textures. An accelerated LoRA module is adopted in the degradation removal stage to mitigate the latent distribution shift between degraded LR images and natural images. The degradation removal stage not only speeds up and reduces the early denoising steps of the reconstruction process, but also aligns

*Corresponding Author.

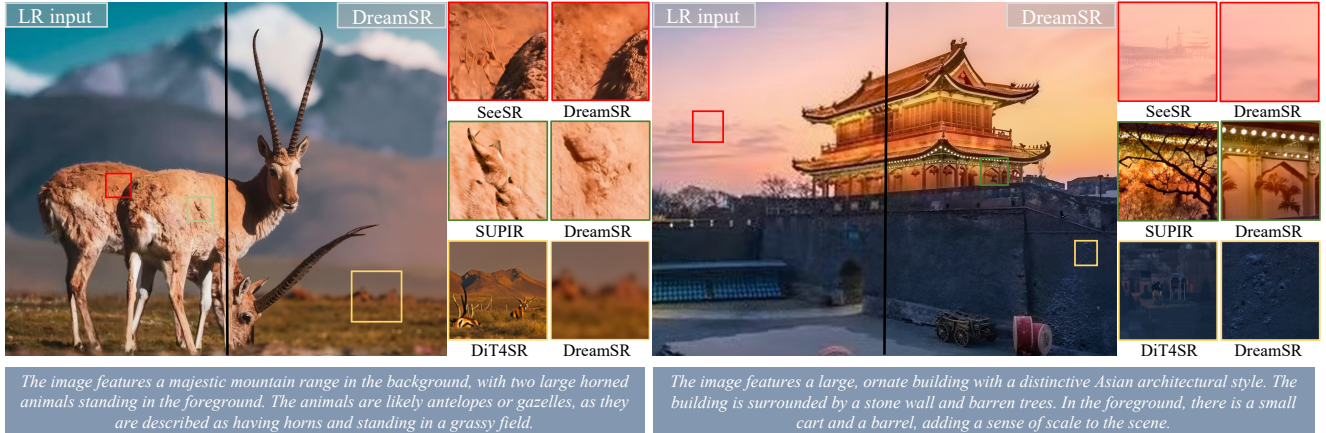


Figure 1. Example of local over-generation in patch-wise inference for high-resolution images. When existing methods adopt patch-wise inference strategy, inconsistent semantic details may appear, due to the misalignment between the global prompt and local patches. On the other hand, the proposed DreamSR can effectively suppresses such artifacts and restores fine-grained textures with high fidelity.

the latent space of LR inputs with that of natural images.

To enhance the model’s performance on generating fine-grained detail in local patches, we introduce a comprehensive training strategy with stage-specific data processing pipelines to improve the generation ability on local features with limited semantics. For the degradation removal stage, we adopt the traditional Real-ESRGAN [57] degradation pipeline. For the texture generation stage, we propose a novel image-to-image degradation pipeline to produce training pairs with substantial texture-level discrepancies, thereby improving the model’s capacity for generating fine-grained details with textural guidance. Additionally, a Receptive-Field Enhancement strategy is introduced to align the feature’s receptive fields during training and inference, further boosting its overall capability.

The contributions of this work are summarized as follows: (i) We present DreamSR, a multi-stage ISR model architected upon pre-trained DiT models. By leveraging their powerful image priors and our specifically designed MM-DiT network architecture, it effectively pushes the performance ceiling of image super-resolution. (ii) We introduce a Patch Context aware MM-ControlNet, which leverages a dual-branch ControlNet to integrate global textual semantics with local patch-level prompts through cross-attention, enabling alignment between patch-level visual features and local textual information, thereby suppressing over-generation in patch regions. (iii) We devise a comprehensive training pipeline that utilizes diverse degradation strategies to increase model performance. The incorporation of a Receptive-Field Enhancement mechanism further enhances the model’s ability to capture fine-grained details during ultra-high-resolution image reconstruction. (iv) We demonstrate through both quantitative and qualitative evaluations that our DreamSR outperforms state-of-the-art methods on real-world datasets with multiple resolutions.

2. Related Work

Image Super-Resolution. Deep learning-based image super-resolution (ISR) methods have achieved remarkable progress in recent years. CNN-based approaches [16, 19, 36, 75, 76] and Transformer-based models [9, 12, 13, 33, 40, 74] have continually advanced the performance upper bound. However, due to the complexity and diversity of real-world degradations, these methods often struggle to effectively remove artifacts and recover fine textures. To mitigate the domain discrepancy between synthetic and real degradations, several studies [57, 72] have focused on learned degradation modeling. Yet, a noticeable gap still remains between synthetically degraded datasets and real-world low-resolution images, leading to suboptimal performance in recovering natural details or enhancing mid-quality real images.

Recently, generative models have been increasingly introduced into ISR to further improve perceptual quality. GAN-based methods [8, 34, 35, 48, 55, 64] significantly enhance the realism of generated details. With the advancement of diffusion models, many approaches [14, 69] have integrated them into SR pipelines, achieving impressive results. Several works [17, 23, 41, 44, 51, 52, 54, 65, 68] employ ControlNet-like structures to incorporate degradation priors, while others introduce semantic cues [7, 15, 30, 31, 38, 42, 49, 50, 58, 62, 67, 71] to exploit the text-image interaction capabilities of text-to-image models, thereby improving detail generation. With the emergence of the Diffusion Transformer (DiT), text-image interaction capabilities have been further strengthened, giving rise to a new wave of DiT-based SR methods. However, these methods generally overlook the crucial alignment between textual information and local image patches at ultra-high resolutions, limiting their ability to fully exploit localized detail generation.

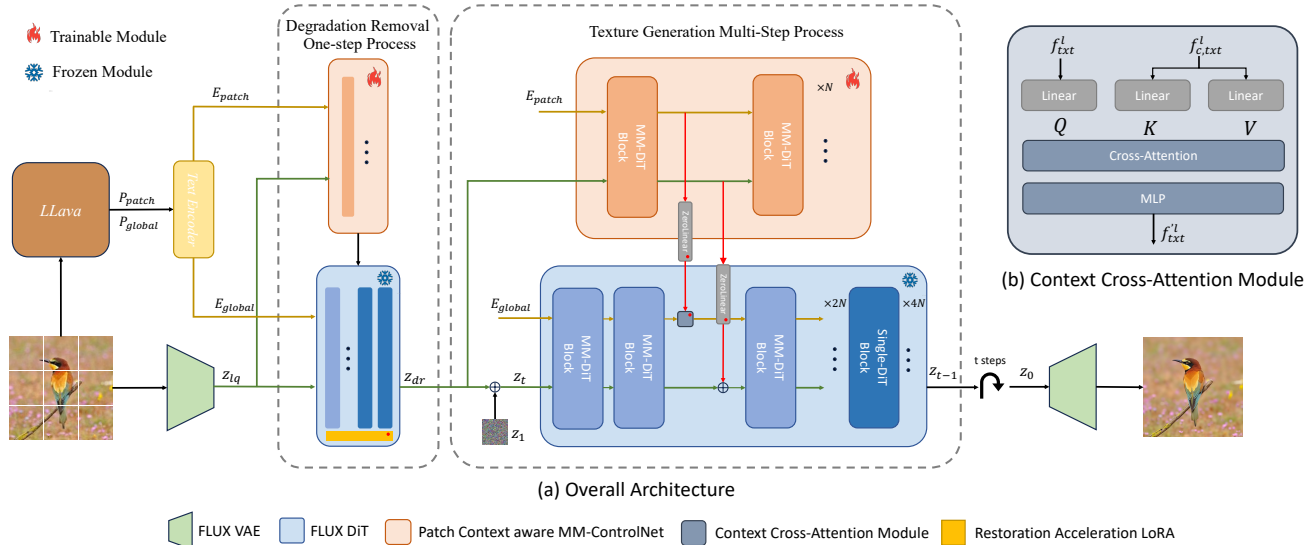


Figure 2. Overview of the proposed DreamSR architecture. Our framework consists of two stages: a degradation removal one-step process and a texture generation process. The Restoration Acceleration LoRA is introduced to compress the early denoising process, while the Patch Context aware MM-ControlNet integrates global and local textual features through the Context Cross-Attention module for effective semantic alignment and fine-grained detail generation.

Diffusion Models. Diffusion models [24] have demonstrated exceptional capability in generating high-quality and diverse natural images. Latent Diffusion Models (LDMs) [46] extend the diffusion process into latent space, greatly improving efficiency while maintaining fidelity in text-to-image synthesis. Through large-scale image-text pretraining, these models effectively capture complex image manifolds and semantic relationships. Several studies [10, 18, 45, 47, 63] have shown that text-to-image diffusion priors outperform GAN-based priors in modeling diverse natural images, motivating their adoption in high-quality super-resolution tasks. More recently, the Diffusion Transformer (DiT) architecture has emerged as a powerful alternative to conventional U-Net backbones, becoming the new mainstream design. In particular, multi-modal variants such as MM-DiT, used in models like FLUX [3] and SD3.0 [22], not only scale model capacity but also strengthen image-text interaction, resulting in more semantically aligned visual outputs. As a result, leveraging such powerful diffusion priors for high-fidelity and controllable image super-resolution has become an active research direction.

3. Methods

We build our DreamSR framework upon Flux.1-dev model [3], aiming to push the performance boundary of image super-resolution by leveraging the powerful pre-trained generative priors of a Diffusion Transformer (DiT). As shown in Figure 2, our DreamSR consists of a fixed DiT,

a Patch Context aware MM-ControlNet and a Restoration Acceleration LoRA [25] module. The reconstruction process is decomposed into two stages: degradation removal and texture generation. In the degradation removal stage, the Restoration Acceleration LoRA module is integrated into the DiT network, which compresses the early-stage denoising process and reduces inference computational cost. In the texture generation stage, the diffusion model (DiT & ControlNet) performs multi-step denoising to synthesize and refine high-frequency textures.

To mitigate the over-generation artifacts that arise from semantic mismatches between local patches and global text during patch-wise inference, we propose a Patch Context aware MM-ControlNet. Unlike previous methods [1] that inject only visual features from ControlNet into DiT, our approach integrates both visual and textual features from the MM-DiT blocks, where local textual information is seamlessly incorporated and effectively combined with global semantics. This design facilitates consistent semantic understanding across patches, ensuring coherent global structures and precise local texture reconstruction.

3.1. Patch Context aware MM-ControlNet

We construct our Patch Context aware MM-ControlNet \mathcal{F}_θ by partially copying the layers from the DiT network ϵ_ϕ in FLUX.1-dev [3]. To enhance the text interaction capability of \mathcal{F}_θ , we selectively employ these text-related blocks (MM-DiT) while discarding Single DiT blocks. These text-related blocks can efficiently process patch-level textual in-

formation and integrate the resulting features into the main network, strengthening its overall capability. Furthermore, to balance restoration performance and inference efficiency, we perform a trimmed replication of the MM-DiT by keeping only half of the MM-DiT blocks in \mathcal{F}_θ . The intermediate features from these blocks are evenly injected into the corresponding MM-DiT blocks of the main network.

During inference, given an LQ image $I_{lq} \in \mathbb{R}^{H \times W \times C}$, we first partition it into overlapping patches $I_{patch} = \{I_{ij} \in \mathbb{R}^{p \times p \times C}\}$ for subsequent patch-wise processing. We use a multi-modal LLM LLaVA [39] to generate both a global prompt P_{global} describing the entire image and localized prompts $P_{patch} = \{P_{ij}\}$ corresponding to individual image patches. During network processing, I_{lq} is first processed by Encoder \mathcal{E} , then gets the latent present \mathbf{z}_{lq} . The patch latent $\mathbf{z}_{lq}^{i,j}$ partitioned from \mathbf{z}_{lq} and local prompt embedding E_{ij} are fed into the MM-ControlNet, while noisy patch latent $\mathbf{z}_t^{i,j}$ partitioned from \mathbf{z}_t and global text prompt embedding E_{global} are injected directly into the DiT network. For a patch latent $\mathbf{z}_{lq}^{i,j}$, the MM-ControlNet outputs a series image features $f_{c,img} = \{f_{c,img}^l\}$ and text features $f_{c,txt} = \{f_{c,txt}^l\}$, $l = 1, \dots, 9$. For each block l , as for the image features, a zero-MLP is used and the feature is directly injected into the main DiT block as

$$f_{img}^l = f_{img}^l + \mathcal{M}^l(f_{c,img}^l), \quad (1)$$

where $\mathcal{M}_{img}^l(\cdot)$ is the zero-MLP layer. As for text features, we introduce a Context Cross-Attention module to enable effective fusion of global and local textual information, which can be defined as

$$f_{txt}^l = \mathcal{M}_{txt}^l(\text{CrossAttention}(Q_{txt}^l, K_{c,txt}^l, V_{c,txt}^l)), \quad (2)$$

where $Q_{txt}^l = P_Q(f_{txt}^l)$, $K_{c,txt}^l = P_K(f_{c,txt}^l)$ and $V_{c,txt}^l = P_V(f_{c,txt}^l)$, $\mathcal{M}_{txt}^l(\cdot)$ is the MLP layer and $P(\cdot)$ represents a linear projection function. This cross-attention mechanism enables dynamic emphasis on the most relevant semantic cues from the global prompt for each local patch while suppressing irrelevant or redundant contextual signals. Consequently, our design facilitates more precise details generation within each local region and preserves the semantic consistency of the overall image.

After obtaining the predicted velocity field $v_p^{i,j}$ for each patch latent $\mathbf{z}_t^{i,j}$ from the network, we follow the same procedure as Multi-Diffusion [2] to aggregate all patch outputs and get v_p , thereby enhancing the global semantic coherence and consistency of the reconstructed image.

3.2. Restoration Acceleration LoRA

Based on the designed model architecture, to increase efficiency when reconstructing high-resolution images, we define a two-stage inference process: degradation removal and

texture generation. Many recent diffusion-based SR methods [1, 37, 67, 68] adopt a degradation removal module to prevent the network from confusing image semantics with degradation information, allowing the main network to focus more on details generation rather than removing image-independent degradation patterns, thereby improving the generative quality and stability of the reconstruction. Inspired by one-step diffusion SR approaches [20, 61], we elegantly integrate the degradation removal process into our network, enabling rapid degradation elimination through a single forward inference while effectively compressing the overall inference process. The restored latent produced in this stage provides a cleaner and more semantically consistent representation, which significantly benefits the subsequent multi-step texture generation phase.

Specifically, during the first inference step, following common practices of the one-step SR model, we augment the DiT network with a Restoration Accelerate LoRA module. The LQ latent \mathbf{z}_{lq} is fed into both the main DiT network and the MM-ControlNet for a single forward pass, producing latent output with degradations removed \mathbf{z}_{dr} . \mathbf{z}_{dr} serves as the condition input for the MM-ControlNet. After getting degradation-removed results, unlike previous methods that still initiate the multi-step generation from pure noise, we utilize \mathbf{z}_{dr} as the intermediate state of the diffusion process. Specifically, the noisy latent \mathbf{z}_t is obtained by injecting controlled Gaussian noise into \mathbf{z}_{dr} as

$$\mathbf{z}_t = (1 - t)\mathbf{z}_{dr} + t \cdot \epsilon, \quad (3)$$

where t is the predefined interpolation step. Starting the diffusion process from this intermediate state \mathbf{z}_t allows the model to bypass redundant early-stage denoising iterations and instead focus on fine-grained texture refinement, efficiently generating high-quality results.

3.3. Training strategy

To address the insufficient detail generation issue, we develop a comprehensive training strategy with stage-specific data processing pipelines, enhancing the model’s sensitivity to local textural guidance. We also develop Receptive-Field Enhancement strategy to align the model’s receptive fields during training and inference, boosting its overall capability. The overall training pipeline is shown in Figure 3.

Stage-specific degradation pipelines. Since the two model stages have distinct priorities, we employ different degradation pipelines to generate training pairs. For the first stage (degradation removal), we use the traditional Real-ESRGAN pipeline [57]. For the second stage (texture generation), we introduce an image-to-image (i2i) degradation method that leverages the FLUX model to erase details from high-quality images, enhancing detail generation through textural guidance. Unlike Real-ESRGAN’s pixel-wise degradation, which compromises both structure and

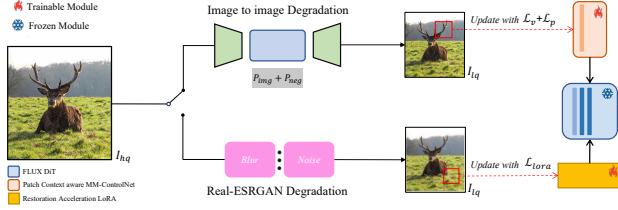


Figure 3. Overall training pipeline for DreamSR.

texture, our i2i approach selectively removes texture details while maintaining global structural consistency. This allows the network to focus on reconstructing high-frequency details with textual guidance, improving output fidelity and realism. Specifically, we start with a high-quality image I_{hq} , an image prompt P_{img} and a negative prompt P_{neg} . After downsampling I_{hq} , we encode it via a VAE encoder to obtain \mathbf{z}_{hq} . This latent representation is blended with Gaussian noise (strength: 0.3–0.5) and then partially denoised using the FLUX model conditioned on $P_{img} + P_{neg}$.

Joint training. During training, we employ a joint optimization strategy to concurrently train the proposed MM-ControlNet and the Restoration Accelerate LoRA module. Specifically, in the initial phase, we first optimize the MM-ControlNet using the datasets generated by the i2i degradation pipeline. The initial training process can stabilize the output. The model typically predicts velocity field v_p and we use velocity loss to update the MM-ControlNet parameters. The velocity loss can be formulated as

$$v_{gt} = \mathbf{z}_1 - \mathbf{z}_0, \quad (4)$$

$$\mathcal{L}_v = \|\mathbf{v}_p - v_{gt}\|_2^2, \quad (5)$$

where $\mathbf{z}_0 = \mathcal{E}(I_{gt})$ is the target latent, \mathbf{z}_1 is the added random noise. In addition, we introduce pixel-level loss to further enhance the reconstruction fidelity. When the sampled t in range $0 \sim 0.2$, we get the prediction output $\hat{\mathbf{z}}_0 = \mathbf{z}_t - tv_p$ and apply it with the VAE Decoder \mathcal{D} into pixel space. Besides \mathcal{L}_v , we additionally use MSE loss and perceptual loss [73] to update the parameter. The pixel loss can be defined as

$$\mathcal{L}_p = \|\mathcal{D}(\hat{\mathbf{z}}_0) - I_{gt}\|_2^2 + \lambda LPIPS(\mathcal{D}(\hat{\mathbf{z}}_0), I_{gt}), \quad (6)$$

where λ is a weighting scalar.

Subsequently, during the iterative training process, the network to be updated is randomly selected at each step. When training the Restoration Acceleration LoRA module for the one-step degradation removal stage, we modify the training objective to image-level loss, directly supervising the model with the ground-truth image. To further enhance perceptual quality, we employ a combination of perceptual loss and GAN loss. Additionally, since the latent output from the one-step process is directly fed into the subsequent multi-step generation stage, a latent-level loss is introduced

to refine the learned representations and ensure consistency across the two stages. The whole loss can be written as

$$\begin{aligned} \mathcal{L}_{lora} = & \|\hat{\mathbf{z}}_{dr} - \mathbf{z}_0\|_2^2 + \|\mathcal{D}(\hat{\mathbf{z}}_{dr}) - I_{gt}\|_2^2 \\ & + \lambda_1 LPIPS(\mathcal{D}(\hat{\mathbf{z}}_{dr}), I_{gt}) + \lambda_2 GAN(\mathcal{D}(\hat{\mathbf{z}}_{dr})), \end{aligned} \quad (7)$$

where λ_1 and λ_2 are weighting scalars. The detailed training schemes are provided in the supplementary material.

Receptive-Field Enhancement training. To enable ultra-high-resolution image restoration, it is crucial to align the data distributions between training and inference. The key lies in the distinction between local and global prompts. Unlike previous approaches that rely on downsampling or randomly cropping large patches (e.g., 768×768 or 1024×1024) from medium-resolution (around 1K resolution) datasets, e.g., LSDIR [32] and FFHQ [27], where local prompts become too similar to global prompts, causing the network to overlook local prompts guidance during reconstruction. So we introduce a Receptive-Field Enhancement training strategy, ensuring sufficient divergence between local and global prompts, thereby reinforcing the importance of local prompt conditions in the reconstruction process. Specifically, we directly extract 512×512 patches from native high-resolution images (mostly around 2K resolution).

4. Experiments

4.1. Datasets and implementation details

Datasets. For training, we utilize a collected dataset consisting of 580,000 high-quality general images and 120,000 face images, each paired with corresponding text descriptions. We pre-generate the corresponding LR counterparts using our i2i degradation pipeline, while the Real-ESRGAN degradation method is also applied online during the training process with the same configuration as SeeSR [62].

Since our method specifically focuses on the Real-ISR task, we evaluate our model on widely used real-world datasets, including RealSR [5], Drealsr [60], RealLR200 [62], RealLQ250 [1] and RealDeg [11] social media subset. Following SeeSR, the LR images from RealSR and Drealsr are center-cropped to 128×128 . RealLR200 contains images ranging from 100×100 to 400×400 , RealLQ250 provides images at 256×256 , and RealDeg includes high-resolution images with a short edge of 720. All experiments are conducted with the scaling factor of $\times 4$.

Evaluation Metrics. In order to comprehensively evaluate the performance of different methods, we employ a suite of both reference-based and no-reference metrics. For reference-based assessment, we utilize PSNR and SSIM [59] to measure reconstruction fidelity, and LPIPS [73] to quantify perceptual quality. For no-reference evaluation, we include MANIQA [66], MUSIQ [28], and CLIPQA+ [53] to assess image quality from diverse perspectives.

Table 1. Quantitative comparison with state-of-the-art methods on real-world image super-resolution benchmarks. The best and second performance are highlighted in red and blue, respectively.

Datasets	Metrics	Methods										
		BSRGAN[72]	Real-ESRGAN[57]	StableSR[54]	DiffBIR[37]	SeeSR[62]	SUPIR[68]	OSDiff[61]	FaithDiff[11]	DreamClear[1]	DiT4SR[21]	Ours
RealSR	PSNR \uparrow	26.3785	25.6855	25.5091	24.8340	25.1465	22.4082	23.3748	24.5681	25.0070	23.5397	20.9305
	SSIM \uparrow	0.7651	0.7614	0.7491	0.6501	0.7210	0.5995	0.7105	0.6927	0.7026	0.6680	0.6058
	LPIPS \downarrow	0.2656	0.2710	0.2604	0.3650	0.3008	0.4204	0.3032	0.2949	0.3258	0.3143	0.4079
	MUSIQ \uparrow	63.2871	60.3671	61.8059	69.2790	69.8241	63.4065	69.2206	68.7046	58.3191	67.5601	70.5560
	MANIQA \uparrow	0.3758	0.3737	0.3769	0.5582	0.5437	0.4472	0.4847	0.4742	0.4313	0.4540	0.5731
	CLIPQA+ \uparrow	0.5822	0.5840	0.6145	0.7233	0.6912	0.5989	0.7200	0.6720	0.5920	0.6609	0.7318
DRealSR	PSNR \uparrow	28.7025	28.6147	29.0182	25.9035	28.0707	24.4641	25.9906	26.2201	28.5904	25.6479	24.0158
	SSIM \uparrow	0.8028	0.8052	0.8044	0.6245	0.7683	0.6198	0.7475	0.6857	0.7532	0.6772	0.6484
	LPIPS \downarrow	0.2858	0.2819	0.2898	0.4669	0.3175	0.4650	0.3138	0.3669	0.3680	0.3745	0.4639
	MUSIQ \uparrow	57.1687	54.2752	51.3571	66.1187	65.0895	62.3864	65.2829	66.5850	43.4771	65.1260	67.3315
	MANIQA \uparrow	0.3403	0.3440	0.3177	0.5543	0.5129	0.4542	0.4765	0.4575	0.3055	0.4425	0.5404
	CLIPQA+ \uparrow	0.5621	0.5546	0.5349	0.7173	0.6792	0.6145	0.7008	0.6686	0.5060	0.6668	0.7028
RealLQ250	MUSIQ \uparrow	63.5230	62.5185	56.6588	67.5315	70.3712	65.9080	69.2500	69.6166	67.1254	71.8311	71.6516
	MANIQA \uparrow	0.3515	0.3565	0.2932	0.4900	0.4894	0.3848	0.4245	0.3971	0.4938	0.4607	0.5319
	CLIPQA+ \uparrow	0.6019	0.6116	0.5709	0.6917	0.7037	0.6542	0.7077	0.6792	0.6922	0.7106	0.7206
RealLR200	MUSIQ \uparrow	64.8724	62.9628	63.2798	66.4224	69.6413	63.8806	69.2590	68.7590	66.3161	70.6282	70.6862
	MANIQA \uparrow	0.3704	0.3689	0.3689	0.4736	0.4698	0.3979	0.4426	0.4268	0.4758	0.4650	0.5488
	CLIPQA+ \uparrow	0.6260	0.6221	0.6409	0.6918	0.7088	0.6418	0.7149	0.6846	0.6912	0.7086	0.7391
RealDeg	MUSIQ \uparrow	43.8358	44.8099	35.5875	40.6098	45.5557	45.5267	44.6909	47.5436	41.8048	44.7736	45.6234
	MANIQA \uparrow	0.3648	0.3848	0.3291	0.4413	0.4535	0.3613	0.4391	0.3862	0.3854	0.4437	0.4574
	CLIPQA+ \uparrow	0.5921	0.6102	0.5358	0.6367	0.6579	0.6094	0.6534	0.6329	0.6290	0.6841	0.6647

Implementation details. Our model is trained on 16 H20 GPUs with a batch size of 64 using AdamW optimizer ($\text{lr}=5\text{e-}6$). During training, images are randomly cropped to 512×512 patches with online-generated local text prompts. The rank of Restoration Acceleration LoRA is set to 256. We first train the MM-ControlNet alone for 20,000 steps to stabilize the output. Subsequently, the model alternates between a multi-step texture generation stage and a single-step degradation removal stage for approximately 100,000 steps. The hyperparameters λ , λ_1 , and λ_2 are set to 2, 2 and 0.5, respectively. To support both patch-based high-resolution restoration and full-image SR for smaller inputs, we resize images to a 1024-pixel shorter side with 0.2 probability while maintaining local text consistency with global text. During inference, we set $t = 0.8$ and the total number of steps to 17, where the first step performs degradation removal and the remaining 16 steps are used for texture generation, resulting in an overall 1+16 inference scheme.

4.2. Comparison with Existing Methods

We compare our method with state-of-the-art Real-ISR methods, including GAN-based methods (i.e. BSRGAN [72], Real-ESRGAN [57]) and diffusion-based methods (i.e. StableSR [54], DiffBIR [37], SeeSR [62], SUPIR [68], OSDiff [61], FaithDiff [11], DreamClear [1], DiT4SR [21]). We use the publicly released codes and models, with default inference configurations for testing.

Quantitative Comparisons. We first show the quantitative comparison on the five real-world datasets in Table 1. It can be seen that our method achieves competitive perfor-

mance on 5 datasets containing various resolutions. For the 128×128 resolution RealSR and DRealSR datasets, our method reaches the best results on non-reference metrics, which reflects the excellent image quality of our results. Due to the inherently strong detail generation capability of diffusion-based models, none of the diffusion-based approaches, including ours, achieves outstanding performance on reference metrics. This phenomenon has also been widely noted in prior studies [4, 26, 68] that existing reference metrics are not suitable for evaluation with the model’s generative ability increasing. On the RealLQ250 and RealLR200 datasets, our method exhibits overwhelming performance, consistently achieving top results across all non-reference metrics. Furthermore, on the high-resolution RealDeg dataset, our model demonstrates excellent objective performance, validating the superiority of our approach in handling high-resolution image reconstruction tasks.

Qualitative Comparisons. The qualitative comparisons against other methods are provided in Figure 4, which clearly demonstrate that our approach generates more natural textures and preserves fine-grained details better than existing methods. For the first two rows, which are sampled from the RealLQ250 dataset with 256×256 low-resolution inputs, our method reconstructs clearer and more plausible details, achieving visually superior results. For the last row, which is selected from the RealDeg dataset with high-resolution outputs, we observe that many competing methods fail to properly recover consistent details due to semantic misalignment during inference, often generating distorted or incorrect textures, while some approaches

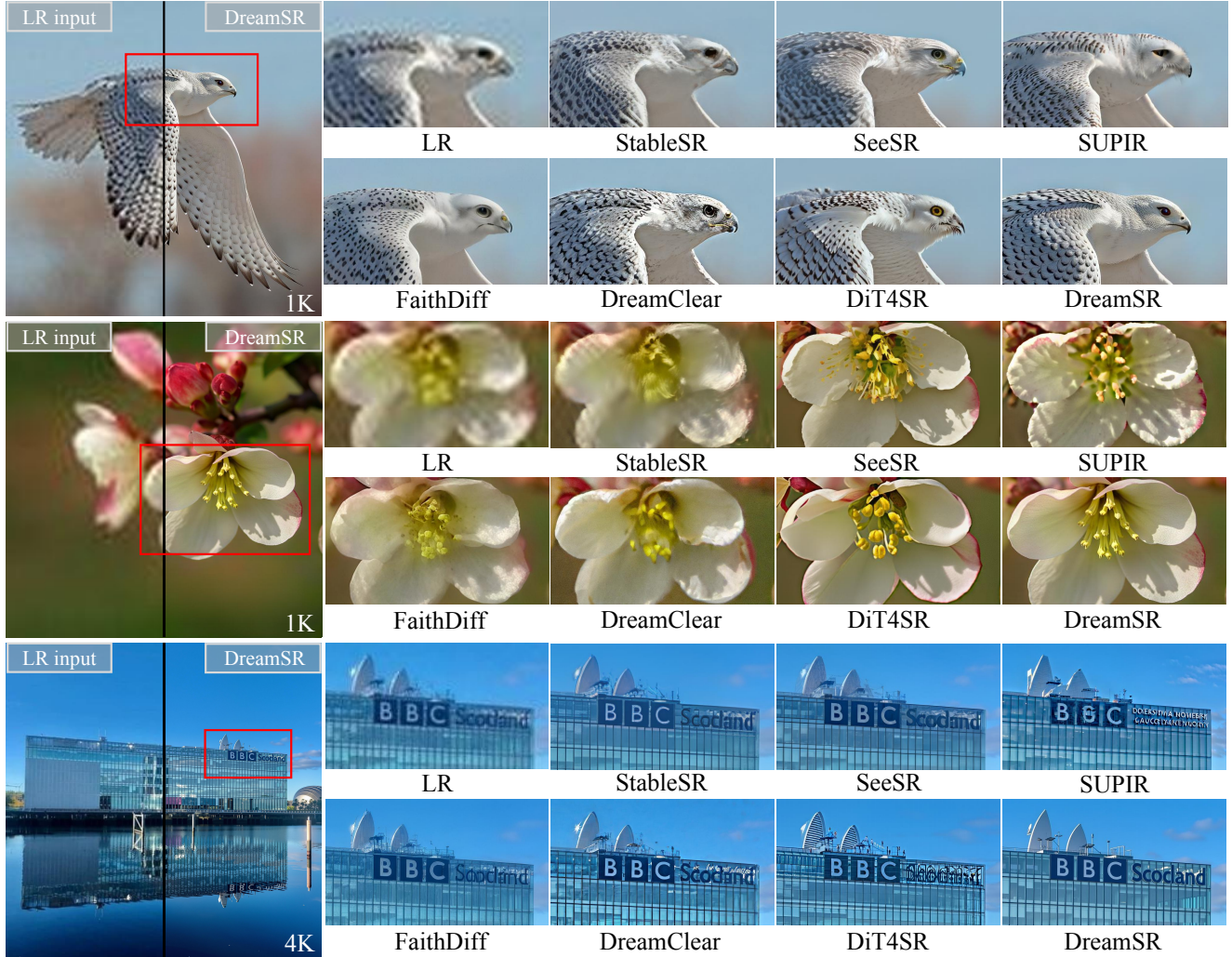


Figure 4. Qualitative comparisons with different methods on real-world datasets. Our DreamSR achieves the best performance, generating more realistic images with fine-scale structures and details. More visual results are included in the supplementary material.

Table 2. Inference-time performance of diffusion-based SR methods for the diffusion process on 2560x1440 resolution images. All methods are tested on a H20 GPU. The best and second performances are highlighted in red and blue, respectively.

	StableSR	DiffBIR	SeeSR	SUPIR	FaithDiff	DreamClear	DiT4SR	Ours
Step	200	50	50	50	20	50	40	1+16
Time (s)	156	127	119	124	30	185	228	86

are unable to produce fine-grained details, leading to overly smooth reconstructions. In contrast, our approach produces structurally coherent and detailed reconstructions, demonstrating its robustness and superior visual fidelity.

Inference time Comparisons. We evaluate the inference efficiency of our model on standard 2K images using a single H20 GPU. Benefiting from our acceleration design, the proposed method achieves high-quality detail reconstruction with only 1+16 inference steps. Our step count is significantly lower than that of other diffusion-based SR meth-

ods. Despite the relatively large parameter size of the DiT architecture, our model still runs faster than most methods built upon SD [46] or SDXL [43] UNet backbones, and is only slower than FaithDiff, which adopts a lightweight design. Overall, our approach achieves a favorable balance between inference speed and reconstruction quality.

4.3. Ablation Study

Effectiveness of dual-branch MM-ControlNet. To validate the effectiveness of the proposed dual-branch MM-ControlNet, we conduct an ablation study by replacing our MM-ControlNet with a conventional ControlNet architecture that removes the text feature branch. The model is trained under the same settings as the full model, except that it uses global prompt. During testing, we evaluate two variants: one using only the global prompt and the other using only patch-level prompts as both DiT and Control-

Table 3. Ablation results of different architectures of ControlNet on RealDeg dataset. After removing the text feature branch of ControlNet, we use different prompt settings to test.

Text branch	Global prompt	Patch prompt	MUSIQ \uparrow	MANIQA \uparrow	CLIPQA+ \uparrow
w/o	✓		41.6816	0.3891	0.6251
w/o		✓	41.5523	0.3932	0.6177
w	✓	✓	45.6234	0.4574	0.6647

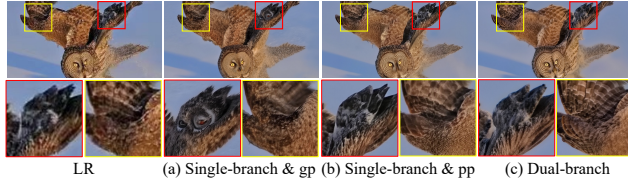


Figure 5. Visual comparison of different prompt configurations. (a) Single-branch ControlNet with global prompt, (b) single-branch ControlNet with patch-level prompt, and (c) our full dual-branch model.

Net inputs. We evaluate the performance on the RealDeg dataset. As shown in Table 3, both variants perform worse than the full version of DreamSR across all metrics. Moreover, qualitative results shown in Figure 5 reveal that when conditioned solely on the global prompt, the model tends to suffer from over-generation artifacts. Conversely, when conditioned only on patch-level prompts, the model lacks sufficient global semantic awareness, leading to unnatural and incoherent textures. These observations demonstrate that our dual-branch ControlNet design effectively enables interaction between global and local textual information through cross-attention, thereby enhancing both semantic consistency and detail generation in reconstructed images.

Effectiveness of Training Strategy. To verify the effectiveness of our proposed training strategy, which includes diverse degradation modeling and Receptive-Field Enhancement training, we conduct ablation experiments on the RealDeg dataset. Specifically, we test two simplified settings: (1) training with only Real-ESRGAN degradation, and (2) removing receptive-field enhancement strategy by resizing the short side of images to 1024 and cropping 1024×1024 patches for training. As shown in Table 4, both ablated settings result in a clear drop across all non-reference metrics, confirming the effectiveness of our full training design. As shown in Figure 6, when only Real-ESRGAN degradation is used, the model fails to reconstruct rich image details resulting in overly smooth and texture-lacking outputs. In contrast, our i2i degradation preserves global structures while introducing stronger local detail variations, effectively improving texture synthesis. Moreover, without the receptive-field enhancement strategy, the model tends to overfit global semantics and leads to degraded reconstruction of local details. These results demonstrate that both training components are crucial for achieving high-quality detail generation in ultra-high-resolution restoration.

Table 4. Ablation results of different training strategies on RealDeg dataset.

Setting	MUSIQ \uparrow	MANIQA \uparrow	CLIPQA+ \uparrow
w/o i2i deg	43.7706	0.3917	0.6355
w/o RFE train	43.5546	0.3868	0.5975
Full setting	45.6234	0.4574	0.6647

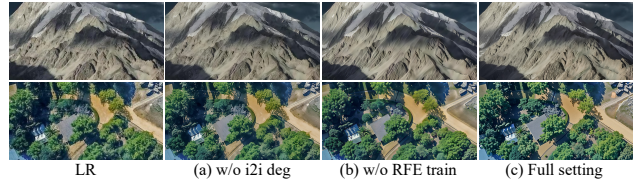


Figure 6. Visual comparison of different training strategies, (a) Without the proposed i2i degradation, (b) without receptive-field enhancement training, and (c) our full model.

Table 5. Ablation results of Restoration Acceleration LoRA on RealDeg dataset. All models are trained using the Real-ESRGAN degradation for fair comparison.

RA LoRA	Inference steps	MUSIQ \uparrow	MANIQA \uparrow	CLIPQA+ \uparrow
w/o	20	37.9976	0.3868	0.5975
w/o	30	38.3402	0.3865	0.6042
w	1+16	43.7706	0.3917	0.6355

Effectiveness of Restoration Acceleration LoRA. To evaluate the effectiveness of the proposed Restoration Acceleration LoRA, we conduct an ablation study by removing the LoRA module and training the model only on the multi-step diffusion stage. It is worth noting that, since different degradation strategies may introduce additional variables affecting the LoRA’s performance, we adopt only the Real-ESRGAN degradation setting for this experiment to ensure a fair comparison. As shown in Table 5, when the LoRA module is removed, even with a larger number of inference steps, the performance consistently lags behind our full multi-stage model across all metrics. This result demonstrates that the proposed LoRA effectively compresses the early-stage denoising process without compromising restoration quality, validating the rationality and efficiency of our two-stage inference framework.

5. Conclusion

In this paper, we introduced DreamSR, a diffusion-based framework for real-world ultra-high-resolution image super-resolution. By addressing the semantic misalignment inherent in patch-wise inference, DreamSR effectively suppresses local over-generation and enhances fine-detail synthesis. Our dual-branch MM-ControlNet integrates global and local textual guidance through cross-attention, achieving consistent semantic alignment between patches and global context. Furthermore, the proposed Receptive Field Enhancement training strategy enables the model to better capture local texture information while maintaining global structural fidelity. Extensive experiments demonstrate that DreamSR achieves state-of-the-art performance and superior perceptual quality on real-world benchmarks.

References

- [1] Yuang Ai, Xiaoqiang Zhou, Huaibo Huang, Xiaotian Han, Zhengyu Chen, Quanzeng You, and Hongxia Yang. Dreamclear: High-capacity real-world image restoration with privacy-safe dataset curation. *Advances in Neural Information Processing Systems*, 37:55443–55469, 2024. [3](#), [4](#), [5](#), [6](#)
- [2] Omer Bar-Tal, Lior Yariv, Yaron Lipman, and Tali Dekel. Multidiffusion: Fusing diffusion paths for controlled image generation. 2023. [1](#), [4](#)
- [3] Black Forest Labs. Flux. <https://github.com/black-forest-labs/flux>, 2024. Accessed: 2024. [1](#), [3](#)
- [4] Yochai Blau and Tomer Michaeli. The perception-distortion tradeoff. In *Proceedings of the IEEE conference on computer vision and pattern recognition*, pages 6228–6237, 2018. [6](#)
- [5] Jianrui Cai, Hui Zeng, Hongwei Yong, Zisheng Cao, and Lei Zhang. Toward real-world single image super-resolution: A new benchmark and a new model. In *Proceedings of the IEEE/CVF international conference on computer vision*, pages 3086–3095, 2019. [5](#)
- [6] Kelvin CK Chan, Xintao Wang, Xiangyu Xu, Jinwei Gu, and Chen Change Loy. Glean: Generative latent bank for large-factor image super-resolution. In *Proceedings of the IEEE/CVF conference on computer vision and pattern recognition*, pages 14245–14254, 2021. [1](#)
- [7] Bin Chen, Gehui Li, Rongyuan Wu, Xindong Zhang, Jie Chen, Jian Zhang, and Lei Zhang. Adversarial diffusion compression for real-world image super-resolution. In *Proceedings of the Computer Vision and Pattern Recognition Conference*, pages 28208–28220, 2025. [2](#)
- [8] Chaofeng Chen, Xinyu Shi, Yipeng Qin, Xiaoming Li, Xiaoguang Han, Tao Yang, and Shihui Guo. Real-world blind super-resolution via feature matching with implicit high-resolution priors. In *Proceedings of the 30th ACM International Conference on Multimedia*, pages 1329–1338, 2022. [2](#)
- [9] Hanting Chen, Yunhe Wang, Tianyu Guo, Chang Xu, Yiping Deng, Zhenhua Liu, Siwei Ma, Chunjing Xu, Chao Xu, and Wen Gao. Pre-trained image processing transformer. In *Proceedings of the IEEE/CVF conference on computer vision and pattern recognition*, pages 12299–12310, 2021. [2](#)
- [10] Junsong Chen, Jincheng Yu, Chongjian Ge, Lewei Yao, Enze Xie, Yue Wu, Zhongdao Wang, James Kwok, Ping Luo, Huchuan Lu, et al. Pixart- α : Fast training of diffusion transformer for photorealistic text-to-image synthesis. *arXiv preprint arXiv:2310.00426*, 2023. [3](#)
- [11] Junyang Chen, Jinshan Pan, and Jiangxin Dong. Faithdiff: Unleashing diffusion priors for faithful image super-resolution. In *Proceedings of the Computer Vision and Pattern Recognition Conference*, pages 28188–28197, 2025. [5](#), [6](#)
- [12] Xiangyu Chen, Xintao Wang, Jiantao Zhou, Yu Qiao, and Chao Dong. Activating more pixels in image super-resolution transformer. In *Proceedings of the IEEE/CVF conference on computer vision and pattern recognition*, pages 22367–22377, 2023. [2](#)
- [13] Zheng Chen, Yulun Zhang, Jinjin Gu, Linghe Kong, Xiaokang Yang, and Fisher Yu. Dual aggregation transformer for image super-resolution. In *Proceedings of the IEEE/CVF international conference on computer vision*, pages 12312–12321, 2023. [2](#)
- [14] Kun Cheng, Lei Yu, Zhijun Tu, Xiao He, Liyu Chen, Yong Guo, Mingrui Zhu, Nannan Wang, Xinbo Gao, and Jie Hu. Effective diffusion transformer architecture for image super-resolution. In *Proceedings of the AAAI Conference on Artificial Intelligence*, pages 2455–2463, 2025. [2](#)
- [15] Qinpeng Cui, Yixuan Liu, Xinyi Zhang, Qiqi Bao, Qingmin Liao, Li Wang, Tian Lu, Zicheng Liu, Zhongdao Wang, and Emad Barsoum. Taming diffusion prior for image super-resolution with domain shift sdes. *arXiv preprint arXiv:2409.17778*, 2024. [2](#)
- [16] Tao Dai, Jianrui Cai, Yongbing Zhang, Shu-Tao Xia, and Lei Zhang. Second-order attention network for single image super-resolution. In *Proceedings of the IEEE/CVF conference on computer vision and pattern recognition*, pages 11065–11074, 2019. [2](#)
- [17] Junyuan Deng, Xinyi Wu, Yongxing Yang, Congchao Zhu, Song Wang, and Zhenyao Wu. Acquire and then adapt: Squeezing out text-to-image model for image restoration. In *Proceedings of the Computer Vision and Pattern Recognition Conference*, pages 23195–23206, 2025. [2](#)
- [18] Prafulla Dhariwal and Alexander Nichol. Diffusion models beat gans on image synthesis. *Advances in neural information processing systems*, 34:8780–8794, 2021. [3](#)
- [19] Chao Dong, Chen Change Loy, Kaiming He, and Xiaoou Tang. Learning a deep convolutional network for image super-resolution. In *European conference on computer vision*, pages 184–199. Springer, 2014. [2](#)
- [20] Linwei Dong, Qingnan Fan, Yihong Guo, Zhonghao Wang, Qi Zhang, Jinwei Chen, Yawei Luo, and Changqing Zou. Tsd-sr: One-step diffusion with target score distillation for real-world image super-resolution. In *Proceedings of the Computer Vision and Pattern Recognition Conference*, pages 23174–23184, 2025. [4](#)
- [21] Zheng-Peng Duan, Jiawei Zhang, Xin Jin, Ziheng Zhang, Zheng Xiong, Dongqing Zou, Jimmy S Ren, Chunle Guo, and Chongyi Li. Dit4sr: Taming diffusion transformer for real-world image super-resolution. In *Proceedings of the IEEE/CVF International Conference on Computer Vision*, pages 18948–18958, 2025. [6](#)
- [22] Patrick Esser, Sumith Kulal, Andreas Blattmann, Rahim Entezari, Jonas Müller, Harry Saini, Yam Levi, Dominik Lorenz, Axel Sauer, Frederic Boesel, et al. Scaling rectified flow transformers for high-resolution image synthesis. In *Forty-first international conference on machine learning*, 2024. [3](#)
- [23] Junhao Gu, Peng-Tao Jiang, Hao Zhang, Mi Zhou, Jinwei Chen, Wenming Yang, and Bo Li. Consissr: Delving deep into consistency in diffusion-based image super-resolution. 2024. [2](#)

- [24] Jonathan Ho, Ajay Jain, and Pieter Abbeel. Denoising diffusion probabilistic models. Advances in neural information processing systems, 33:6840–6851, 2020. 3
- [25] Edward J Hu, Yelong Shen, Phillip Wallis, Zeyuan Allen-Zhu, Yuanzhi Li, Shean Wang, Lu Wang, Weizhu Chen, et al. Lora: Low-rank adaptation of large language models. ICLR, 1(2):3, 2022. 3
- [26] Gu Jinjin, Cai Haoming, Chen Haoyu, Ye Xiaoxing, Jimmy S Ren, and Dong Chao. Pipal: a large-scale image quality assessment dataset for perceptual image restoration. In European conference on computer vision, pages 633–651. Springer, 2020. 6
- [27] Tero Karras, Samuli Laine, and Timo Aila. A style-based generator architecture for generative adversarial networks. In Proceedings of the IEEE/CVF conference on computer vision and pattern recognition, pages 4401–4410, 2019. 5
- [28] Junjie Ke, Qifei Wang, Yilin Wang, Peyman Milanfar, and Feng Yang. Musiq: Multi-scale image quality transformer. In Proceedings of the IEEE/CVF international conference on computer vision, pages 5148–5157, 2021. 5
- [29] Christian Ledig, Lucas Theis, Ferenc Huszár, Jose Caballero, Andrew Cunningham, Alejandro Acosta, Andrew Aitken, Alykhan Tejani, Johannes Totz, Zehan Wang, et al. Photo-realistic single image super-resolution using a generative adversarial network. In Proceedings of the IEEE conference on computer vision and pattern recognition, pages 4681–4690, 2017. 1
- [30] Jianze Li, Jiezhong Cao, Zichen Zou, Xiongfei Su, Xin Yuan, Yulun Zhang, Yong Guo, and Xiaokang Yang. Distillation-free one-step diffusion for real-world image super-resolution. 2024. 2
- [31] Jianze Li, Jiezhong Cao, Yong Guo, Wenbo Li, and Yulun Zhang. One diffusion step to real-world super-resolution via flow trajectory distillation. arXiv preprint arXiv:2502.01993, 2025. 2
- [32] Yawei Li, Kai Zhang, Jingyun Liang, Jiezhong Cao, Ce Liu, Rui Gong, Yulun Zhang, Hao Tang, Yun Liu, Denis Demandolx, et al. Lsdir: A large scale dataset for image restoration. In Proceedings of the IEEE/CVF Conference on Computer Vision and Pattern Recognition, pages 1775–1787, 2023. 5
- [33] Jingyun Liang, Jiezhong Cao, Guolei Sun, Kai Zhang, Luc Van Gool, and Radu Timofte. Swinir: Image restoration using swin transformer. In Proceedings of the IEEE/CVF international conference on computer vision, pages 1833–1844, 2021. 2
- [34] Jie Liang, Hui Zeng, and Lei Zhang. Details or artifacts: A locally discriminative learning approach to realistic image super-resolution. In Proceedings of the IEEE/CVF conference on computer vision and pattern recognition, pages 5657–5666, 2022. 2
- [35] Jie Liang, Hui Zeng, and Lei Zhang. Efficient and degradation-adaptive network for real-world image super-resolution. In European Conference on Computer Vision, pages 574–591. Springer, 2022. 2
- [36] Bee Lim, Sanghyun Son, Heewon Kim, Seungjun Nah, and Kyoung Mu Lee. Enhanced deep residual networks for single image super-resolution. In Proceedings of the IEEE conference on computer vision and pattern recognition workshops, pages 136–144, 2017. 2
- [37] Xinqi Lin, Jingwen He, Ziyang Chen, Zhaoyang Lyu, Bo Dai, Fanghua Yu, Yu Qiao, Wanli Ouyang, and Chao Dong. Diffbir: Toward blind image restoration with generative diffusion prior. In European conference on computer vision, pages 430–448. Springer, 2024. 4, 6
- [38] Xinqi Lin, Fanghua Yu, Jinfan Hu, Zhiyuan You, Wu Shi, Jimmy S Ren, Jinjin Gu, and Chao Dong. Harnessing diffusion-yielded score priors for image restoration. arXiv preprint arXiv:2507.20590, 2025. 2
- [39] Haotian Liu, Chunyuan Li, Qingyang Wu, and Yong Jae Lee. Visual instruction tuning. Advances in neural information processing systems, 36:34892–34916, 2023. 4
- [40] Yong Liu, Hang Dong, Boyang Liang, Songwei Liu, Qingji Dong, Kai Chen, Fangmin Chen, Lean Fu, and Fei Wang. Unfolding once is enough: A deployment-friendly transformer unit for super-resolution. In Proceedings of the 31st ACM international conference on multimedia, pages 7952–7960, 2023. 2
- [41] Yong Liu, Hang Dong, Jinshan Pan, Qingji Dong, Kai Chen, Rongxiang Zhang, Lean Fu, and Fei Wang. Patchscaler: An efficient patch-independent diffusion model for image super-resolution. In Proceedings of the IEEE/CVF International Conference on Computer Vision, pages 11283–11293, 2025. 2
- [42] Mehdi Noroozi, Isma Hadji, Brais Martinez, Adrian Bulat, and Georgios Tzimiropoulos. You only need one step: Fast super-resolution with stable diffusion via scale distillation. In European Conference on Computer Vision, pages 145–161. Springer, 2024. 2
- [43] Dustin Podell, Zion English, Kyle Lacey, Andreas Blattmann, Tim Dockhorn, Jonas Müller, Joe Penna, and Robin Rombach. Sdxl: Improving latent diffusion models for high-resolution image synthesis. arXiv preprint arXiv:2307.01952, 2023. 1, 7
- [44] Yunpeng Qu, Kun Yuan, Kai Zhao, Qizhi Xie, Jinhua Hao, Ming Sun, and Chao Zhou. Xpsr: Cross-modal priors for diffusion-based image super-resolution. In European Conference on Computer Vision, pages 285–303. Springer, 2024. 2
- [45] Aditya Ramesh, Prafulla Dhariwal, Alex Nichol, Casey Chu, and Mark Chen. Hierarchical text-conditional image generation with clip latents. arXiv preprint arXiv:2204.06125, 1(2):3, 2022. 3
- [46] Robin Rombach, Andreas Blattmann, Dominik Lorenz, Patrick Esser, and Björn Ommer. High-resolution image synthesis with latent diffusion models. In Proceedings of the IEEE/CVF conference on computer vision and pattern recognition, pages 10684–10695, 2022. 3, 7
- [47] Chitwan Saharia, William Chan, Saurabh Saxena, Lala Li, Jay Whang, Emily L Denton, Kamyar Ghasemipour, Raphael Gontijo Lopes, Burcu Karagol Ayan, Tim Salimans, et al. Photorealistic text-to-image diffusion models with deep language understanding. Advances in neural information processing systems, 35:36479–36494, 2022. 3
- [48] Haoze Sun, Wenbo Li, Jianzhuang Liu, Haoyu Chen, Renjing Pei, Xueyi Zou, Youliang Yan, and Yujiu Yang. Coser:

- Bridging image and language for cognitive super-resolution. In Proceedings of the IEEE/CVF Conference on Computer Vision and Pattern Recognition, pages 25868–25878, 2024. 2
- [49] Lingchen Sun, Rongyuan Wu, Zhengqiang Zhang, Hongwei Yong, and Lei Zhang. Improving the stability of diffusion models for content consistent super-resolution. CoRR, 2024. 2
- [50] Lingchen Sun, Rongyuan Wu, Zhiyuan Ma, Shuaizheng Liu, Qiaosi Yi, and Lei Zhang. Pixel-level and semantic-level adjustable super-resolution: A dual-lora approach. In Proceedings of the Computer Vision and Pattern Recognition Conference, pages 2333–2343, 2025. 2
- [51] Li-Yuan Tsao, Hao-Wei Chen, Hao-Wei Chung, Deqing Sun, Chun-Yi Lee, Kelvin CK Chan, and Ming-Hsuan Yang. Holisdip: Image super-resolution via holistic semantics and diffusion prior. arXiv preprint arXiv:2411.18662, 2024. 2
- [52] Yuhao Wan, Peng-Tao Jiang, Qibin Hou, Hao Zhang, Jinwei Chen, Ming-Ming Cheng, and Bo Li. Clearsr: Latent low-resolution image embeddings help diffusion-based real-world super resolution models see clearer. 2024. 2
- [53] Jianyi Wang, Kelvin CK Chan, and Chen Change Loy. Exploring clip for assessing the look and feel of images. In Proceedings of the AAAI conference on artificial intelligence, pages 2555–2563, 2023. 5
- [54] Jianyi Wang, Zongsheng Yue, Shangchen Zhou, Kelvin CK Chan, and Chen Change Loy. Exploiting diffusion prior for real-world image super-resolution. International Journal of Computer Vision, 132(12):5929–5949, 2024. 2, 6
- [55] Xintao Wang, Ke Yu, Shixiang Wu, Jinjin Gu, Yihao Liu, Chao Dong, Yu Qiao, and Chen Change Loy. Esgan: Enhanced super-resolution generative adversarial networks. In Proceedings of the European conference on computer vision (ECCV) workshops, pages 0–0, 2018. 2
- [56] Xintao Wang, Yu Li, Honglun Zhang, and Ying Shan. Towards real-world blind face restoration with generative facial prior. In Proceedings of the IEEE/CVF conference on computer vision and pattern recognition, pages 9168–9178, 2021. 1
- [57] Xintao Wang, Liangbin Xie, Chao Dong, and Ying Shan. Real-esrgan: Training real-world blind super-resolution with pure synthetic data. In Proceedings of the IEEE/CVF international conference on computer vision, pages 1905–1914, 2021. 2, 4, 6
- [58] Yufei Wang, Wenhan Yang, Xinyuan Chen, Yaohui Wang, Lanqing Guo, Lap-Pui Chau, Ziwei Liu, Yu Qiao, Alex C Kot, and Bihan Wen. Sinsr: diffusion-based image super-resolution in a single step. In Proceedings of the IEEE/CVF conference on computer vision and pattern recognition, pages 25796–25805, 2024. 2
- [59] Zhou Wang, Alan C Bovik, Hamid R Sheikh, and Eero P Simoncelli. Image quality assessment: from error visibility to structural similarity. IEEE transactions on image processing, 13(4):600–612, 2004. 5
- [60] Pengxu Wei, Ziwei Xie, Hannan Lu, Zongyuan Zhan, Qixiang Ye, Wangmeng Zuo, and Liang Lin. Component divide-and-conquer for real-world image super-resolution. In European conference on computer vision, pages 101–117. Springer, 2020. 5
- [61] Rongyuan Wu, Lingchen Sun, Zhiyuan Ma, and Lei Zhang. One-step effective diffusion network for real-world image super-resolution. Advances in Neural Information Processing Systems, 37:92529–92553, 2024. 4, 6
- [62] Rongyuan Wu, Tao Yang, Lingchen Sun, Zhengqiang Zhang, Shuai Li, and Lei Zhang. Seesr: Towards semantics-aware real-world image super-resolution. In Proceedings of the IEEE/CVF conference on computer vision and pattern recognition, pages 25456–25467, 2024. 2, 5, 6
- [63] Enze Xie, Junsong Chen, Junyu Chen, Han Cai, Haotian Tang, Yujun Lin, Zhekai Zhang, Muyang Li, Ligeng Zhu, Yao Lu, et al. Sana: Efficient high-resolution image synthesis with linear diffusion transformers. arXiv preprint arXiv:2410.10629, 2024. 3
- [64] Liangbin Xie, Xintao Wang, Xiangyu Chen, Gen Li, Ying Shan, Jiantao Zhou, and Chao Dong. Desra: detect and delete the artifacts of gan-based real-world super-resolution models. arXiv preprint arXiv:2307.02457, 2023. 2
- [65] Rui Xie, Chen Zhao, Kai Zhang, Zhenyu Zhang, Jun Zhou, Jian Yang, and Ying Tai. Addr: Accelerating diffusion-based blind super-resolution with adversarial diffusion distillation. arXiv preprint arXiv:2404.01717, 2024. 2
- [66] Sidi Yang, Tianhe Wu, Shuwei Shi, Shanshan Lao, Yuan Gong, Mingdeng Cao, Jiahao Wang, and Yujiu Yang. Maniqa: Multi-dimension attention network for no-reference image quality assessment. In Proceedings of the IEEE/CVF conference on computer vision and pattern recognition, pages 1191–1200, 2022. 5
- [67] Tao Yang, Rongyuan Wu, Peiran Ren, Xuansong Xie, and Lei Zhang. Pixel-aware stable diffusion for realistic image super-resolution and personalized stylization. In European conference on computer vision, pages 74–91. Springer, 2024. 2, 4
- [68] Fanghua Yu, Jinjin Gu, Zheyuan Li, Jinfan Hu, Xiangtao Kong, Xintao Wang, Jingwen He, Yu Qiao, and Chao Dong. Scaling up to excellence: Practicing model scaling for photo-realistic image restoration in the wild. In Proceedings of the IEEE/CVF conference on computer vision and pattern recognition, pages 25669–25680, 2024. 1, 2, 4, 6
- [69] Zongsheng Yue, Jianyi Wang, and Chen Change Loy. Resshift: Efficient diffusion model for image super-resolution by residual shifting. Advances in Neural Information Processing Systems, 36:13294–13307, 2023. 2
- [70] Zongsheng Yue, Jianyi Wang, and Chen Change Loy. Efficient diffusion model for image restoration by residual shifting. IEEE Transactions on Pattern Analysis and Machine Intelligence, 2024. 1
- [71] Aiping Zhang, Zongsheng Yue, Renjing Pei, Wenqi Ren, and Xiaochun Cao. Degradation-guided one-step image super-resolution with diffusion priors. arXiv preprint arXiv:2409.17058, 2024. 2
- [72] Kai Zhang, Jingyun Liang, Luc Van Gool, and Radu Timofte. Designing a practical degradation model for deep blind image super-resolution. In Proceedings of the IEEE/CVF international conference on computer vision, pages 4791–4800, 2021. 2, 6

- [73] Richard Zhang, Phillip Isola, Alexei A Efros, Eli Shechtman, and Oliver Wang. The unreasonable effectiveness of deep features as a perceptual metric. In Proceedings of the IEEE conference on computer vision and pattern recognition, pages 586–595, 2018. [5](#)
- [74] Xindong Zhang, Hui Zeng, Shi Guo, and Lei Zhang. Efficient long-range attention network for image super-resolution. In European conference on computer vision, pages 649–667. Springer, 2022. [2](#)
- [75] Yulun Zhang, Kunpeng Li, Kai Li, Lichen Wang, Bineng Zhong, and Yun Fu. Image super-resolution using very deep residual channel attention networks. In Proceedings of the European conference on computer vision (ECCV), pages 286–301, 2018. [2](#)
- [76] Yulun Zhang, Yapeng Tian, Yu Kong, Bineng Zhong, and Yun Fu. Residual dense network for image super-resolution. In Proceedings of the IEEE conference on computer vision and pattern recognition, pages 2472–2481, 2018. [2](#)